Molecular Dynamics Simulation of Fullerene C_{60} in Ethanol Solution

Zhen Cao,[†] Yuxing Peng,[†] Shu Li,[†] Lei Liu,[†] and Tianying Yan*[,‡]

Institute of New Energy Material Chemistry, Department of Material Chemistry, Nankai University, Tianjin 300071, China, and Institute of Scientific Computing, Nankai University, Tianjin 300071, China

Received: July 4, 2008; Revised Manuscript Received: November 5, 2008

An ethanol solution containing one or two fullerene C_{60} molecules was studied via molecular dynamics simulation. We found that the ethanol molecules form several solvation shells around the central fullerene molecule. Radial distribution functions (RDFs) and hydrogen-bond analyses were employed to detect the structure of the ethanol molecules in the solvation shells. The ethanol molecules in the first solvation shell tend to have their nonpolar alkyl groups exposed to the C_{60} surface while the polar hydroxyl groups point outward to maintain a hydrogen-bond network with a clathrate-like structure. Such orientation of the ethanol molecules in the first solvation shell modulates the orientation of the ethanol molecules in the second solvation shell to have the hydroxyl groups pointing inward. The potential of mean force (PMF) between two C_{60} molecules in ethanol solution showed that C_{60} molecules tend to aggregate in the ethanol solution. There is no ethanol molecule in the intersolute area if the distance between the centers of mass of two C_{60} molecules is shorter than 10.2 Å. The ethanol molecules near the intersolute area tend to have their methyl groups penetrating into the intersolute region if the distance between two C_{60} molecules is short, although the hydroxyl groups have smaller volume. We analyzed the dynamic properties of the ethanol molecules in different solvation shells and found that the relaxation is much slower than that of water solution of C_{60} molecules. In addition, the relaxation of the first solvation shell is slower than that in other solvation shells. The lifetime of the hydrogen-bond in the first solvation shell is also longer than that in other solvation shells while the reorientation of the hydrogen-bonded ethanol pair contributes little to break the hydrogen-bonds.

1. Introduction

The study of the controllable synthesis and manipulation of nanomaterial based on fullerene C_{60} is attractive because it is applicable in many fields. Addition of C_{60} into traditional polymers,[1] inorganic porous materials,[2] and organic supermolecules[3,4] can adjust the structure and improve the properties of these materials. At the same time, people found that the fullerene C_{60} molecules have special applications in biochemical systems, such as inhibiting HIV protease,[5,6] cleaving DNA,[7] and delivering drugs.[8] However, the solubility of the fullerene is still a challenge for further application in separation and assembly.[9] The potential toxicity also limits its addition into medicine.[10] Functionalization of the fullerene molecules with hydrophilic groups is a straightforward way to solve this problem.[11,12] In the meantime, modification of the fullerene without a direct covalent bond has also been reported,[9] with the main purpose to produce metastable dispersed fullerene particles in solution. The method of manipulation of the dispersed fullerene was also widely applied in the synthesis of the fullerene derivatives in different kinds of solutions.[11,12]

Investigations directed to understand the microscopic processes responsible for the formation of dispersed systems have emphasized the role of hydrophobic interactions.[13−16] It is generally accepted that the hydrophobic solutes exclude water molecules and form cavities in aqueous solution while the surrounding water molecules enwrap these cavities and form clathrate-like structures on a certain scale.[17−20] The interface between the cavities and the surrounding water molecules distinguishes the dispersed structures, such as micelles, bilayers, or microemulsions, from the bulk solvent by the ordered structure,[18] leading to lower entropy, offset by the enthalpy effect.[21] It was earlier reported that the hydrogen-bonds are enhanced near a small hydrophobic solute but broken near a large hydrophobic one.[22] Therefore, a large hydrophobic solute induces solvation structures different from that of a small hydrophobic solute. It is also notable that the hydrophobic solute fullerene C_{60} is widely employed as a prototype in the molecular dynamics simulations to understand the hydrophobic effect. Detailed structural and dynamic properties of C_{60} in water have been explored by both the all-atom model[23] and coarse-grained model.[24,25] In order to investigate the aggregate of C_{60} in water, free energy calculations were performed,[26,27] and it was reported that water molecules contribute to the repulsion between the C_{60} molecules.[27] In addition, the geometrical structure of the C_{60} cluster in water was also explored for the purpose of understanding the morphology of the C_{60} particles in aqueous solution.[28]

Compared with the water molecule, the amphiphilic alcohol molecules, such as ethanol, have in particular a nonpolar tail as well as a polar head. The polar heads make the behavior of the solvent molecules similar to that of the water solution. However, the nonpolar tail, an alkyl group for the alcohol, causes the properties and behavior of the ethanol molecules to be different from those of water. For example, ethanol forms two hydrogen-bonds per molecule,[29,30] which is less than the number of hydrogen-bonds formed per water. It makes the boiling point of the alcohol lower than that of water. With the elongation of the alkyl group, the differences between the alcohol and water become even greater. It was reported that the relative volume

* To whom correspondence should be addressed. Tel.: (86)22-2350-5382, fax: (86)22-2350-2604, e-mail: tyan@nankai.edu.cn.
[†] Institute of New Energy Material Chemistry.
[‡] Institute of Scientific Computing.

10.1021/jp805894g CCC: $40.75
Published on Web 12/11/2008

of the solute may affect the scale of the ordered solution structure.[18−21] The increment of the volume of the solvent molecule may also affect the scale of the ordered structure of solvation shells. Therefore, it is of interest to study the interaction between the hydrophobic C_{60} surface and alkyl group of the ethanol molecule and its inducement to the solvation structure. There is few simulation work[31] on the detailed structure of the alcohol molecules around the target hydrophobic solute, although the alcohol solution has been largely applied in the synthesis and manipulation of fullerene particles. For example, alcohol solutions were utilized in the preparation of dispersed nanotubes, which could be used as electronic devices.[11,32] It was also reported that a C_{60} nanosheet was synthesized in the interface between CCl_4 and different kinds of alcohols.[33] Recently, it was found that the tendency of fullerene C_{60} to form a nanocluster is strong in polar media, and the dispersed C_{60} cluster is very stable under this condition.[34−37]

In this study, we report the structure and dynamics of the solvation shells of ethanol around a target fullerene C_{60}, as well as the potential of mean force (PMF) of two C_{60} molecules in ethanol solution. The detailed solvation shells around the target fullerene C_{60} in a simple amphiphilic solvent, ethanol, is studied via molecular dynamic (MD) simulation. It may be useful not only in the explanation of the stability of the dispersed C_{60} in ethanol compared to water but also in further design of suitable solvents for the application of fullerenes. The different arrangements of the polar and nonpolar groups around the C_{60} molecule due to the hydrophobicity of the target fullerene molecule may provide further insights into the solvation and aggregation of fullerenes.

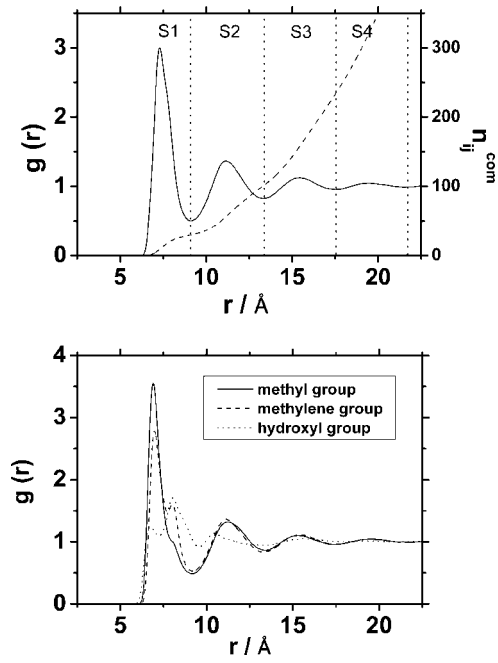

Figure 1. Radial distribution functions (RDFs) of an ethanol solution containing one C_{60}. The RDF of the center of mass (COM) of C_{60} to the COM of ethanol (a), and to the individual functional groups of ethanol (b). The dashed line in part a is the cumulative distribution function of the ethanol molecules versus distance from the COM of fullerene and ethanol. The geometrical definition of solvation shells is from the surface of C_{60} to the first minimum in the RDF (S1), the area between the first and second minima (S2), the area between the second and third minima (S3), and the area between the third and forth minima (S4). The dotted line in part a is a guide for the eye.

2. Simulation Method

Classical molecular dynamics simulation of the system consisting of 1024 ethanol molecules and 1 fullerene C_{60} was performed with GROMACS.[38] We employed the OPLS force field[39] for the ethanol, and the C_{60} molecule is simulated as an uncharged sphere interacting with the Lennard−Jones (LJ) potential corresponding to the sp^2 hybrid carbon atoms in the AMBER force field.[40] SHAKE algorithm[41] was applied to fix all of the C−H bonds and the O−H bond of the ethanol molecules, as well as the C−C bonds of the C_{60} molecule. Thus, C_{60} was treated as a rigid ball in this simulation. The LJ potential was used to treat all the ethanol−ethanol, C_{60}−ethanol, and C_{60}−C_{60} interactions, with the parameters obtained from combination rule $\varepsilon_{ij} = (\varepsilon_i\varepsilon_j)^{1/2}$ and $\sigma_{ij} = (\sigma_i + \sigma_j)/2$. This combination rule was also used in the previous simulations of water and planar hydrophobic solute.[42,43] LJ and real space electrostatic interactions were cut off at 12 Å, and the particle-mesh Ewald (PME) algorithm[44] was applied to handle the long-range electrostatics interactions in reciprocal space. The model systems were maintained at constant temperature of 300 K and pressure of 1.0 bar with using the Berendsen algorithm[45] with periodic boundary conditions (PBC). The integration time step was 2 fs. For a target C_{60} molecule in 1024 ethanol molecules, the simulation started with NPT simulation for 1 ns as equilibration and then 10 ns NPT simulation performed for the production run. The potential of mean force (PMF) of two C_{60} molecules in 1024 ethanol molecules was determined by integrating the mean force acting on two C_{60} molecules. We performed 56 simulations with different distances, ranging from 9.2 Å to 20.2 Å, with a 0.2 Å interval, between the centers of mass (COM) distance of two C_{60} molecules. In each PMF simulation, the system was equilibrated for 1.0 ns and sampled for another 2.0 ns. Monte-Carlo simulation was applied to calculate the PMF of two C_{60} molecules in vacuum.

3. Results and Discussion

3.1. Liquid Structure around the Target C_{60}. Figure 1a and 1b show the radial distribution functions (RDFs), $g(r)$, between the COM of C_{60} and the COM of ethanol, as well as the individual functional groups of ethanol molecules, respectively. Four solvation shells, i.e., S1 to S4, are identified with the geometrical criteria from the minima in the COM RDF shown in Figure 1a. A striking feature of the RDF is the oscillation that extends to over 20 Å, approaching half of the PBC box length. Such oscillation is much more intense than the RDFs of C_{60}−water system found in previous molecular dynamics (MD) simulations,[21,23,25,46] as well as the experiment of the C_{60}−anion in potassium ammonia solution.[47] The dashed line in Figure 1a shows the cumulative distribution function (CDF) of COM of ethanol molecules around the central C_{60}. CDF is related to RDF with $n(r) = \int \rho r 4\pi r'^2 g(r')\mathrm{d}r'$, in which ρ denotes the average number density of ethanol. S1 contains about 30 ethanol molecules, which is comparable to Malaspina's MD simulation of ethanol and C_{60}.[31] It is notable that the geometrically optimized C_{60}−H_2O clathrate-like structures with either ab initio calculation[48] or empirical force field[49] show an optimized water cluster which consists of 60 H_2O molecules enwrapping one C_{60} molecule. Thus, the relative volume of C_{60} compared with water is larger, as expected. It was reported that the solvation structure depends much on the relative volume of the hydrophobic solute, and the smaller hydrophobic solute induces less extended ordered structure in aqueous solution.[18−21] However, the spatial correlation of the ethanol solvation shells around the C_{60} is much more extended in this simulation. The

result may be partially attributed to that a local ordered structure that is induced by the central C_{60} molecule, within which the ethanol molecules almost have a mono-orientational structure that induces far more extended solvation shells compared with water. As shown in Figure 1b for the RDFs between the COM of C_{60} and the individual functional groups of the ethanol molecules, the main peak of the hydroxyl group is further from the COM of C_{60} than the peak representing the alkyl groups. The low peaks for the hydroxyl group at ~6.5 Å to the central C_{60} does not show this main tendency because from the CDF there are few ethanol molecules within this distance. Therefore, most of the ethanol molecules in S1 tend to slant toward the C_{60} surface with the alkyl groups exposed to the C_{60} molecule while the hydroxyl groups point outward from the C_{60} molecule. Because of the hydrophobic nature of C_{60}, the nonpolar tails, rather than polar heads of the ethanol molecules, tend to expose themselves to the nonpolar C_{60} surface. The curvature of the C_{60} makes it difficult for the adjacent hydroxyl groups of ethanol to maintain a complete hydrogen-bond network with the surrounding liquid molecules at the surface of C_{60}, if the hydroxyl groups are too close to C_{60} molecule. So the hydroxyl groups of the ethanol molecules are repelled from the C_{60} surface and form a hydrogen-bond network at the outer boundary of S1. The outer hydroxyl groups form a hydrogen-bond network with the molecules in the first solvation shell as well as with the molecules in S2. Such structure stabilizes the fullerene molecules in the solution by screening it with a polar clathrate-like framework near the central C_{60}. Apart from the preferred orientation of the ethanol molecules in S1, a few ethanol molecules take an opposite orientation with the hydroxyl group exposed to C_{60} and the methyl group pointing outward. Such arrangement can be seen in Figure 1b for the weak hydroxyl peak at ca. 7 Å, which correlates to the weak second methyl and methylene peaks around 1 Å from their individual main peaks.

The interactions between the ethanol molecules in S1 and C_{60} induce three additional solvation shells, as shown in Figure 1a. The ethanol molecules in the outer solvation shells rearrange themselves to correlate with those in the inner solvation shell. The amphiphilic structure of ethanol makes such a correlation notable for the extended structure. It can be observed in Figure 1b that the main peak of the hydroxyl group in S2 is much closer compared with the peak in S1. The detailed orientational distribution of the ethanol molecules around the central C_{60} is shown in Figure 2a of the two-dimensional RDF, $g(r, \cos\theta)$, in which θ is the angle between the dipole moment of the ethanol and the vector from COM of C_{60} to the COM of ethanol. Ethanol molecules in S1 surrounding the central C_{60} show a narrow distribution compared with water surrounding C_{60} and are similar to water surrounding CH_4.[21] This peak can be interpreted as the dipole moment of ethanol, which is mainly pointing toward the C_{60} surface in S1. Considering the individual functional group RDFs shown in Figure 1b in which the ethanol molecules tend to have their hydroxyl groups pointing outward, we find some of the ethanol molecules in S1 tend to have the oxygen atoms exposed to the outer ethanol molecules. These oxygen atoms act as the hydrogen-bond acceptors. The orientational distribution of the ethanol molecules in S2 is relatively broad, and the main peak locates at $0.6 < \cos\theta < 0.8$. This detailed distribution indicates that the ethanol molecules in S2 tend to reorientate themselves to have their hydrogen atoms pointing inward and acting as hydrogen-bond donors, though this tendency is not very significant. Such reorganization of the

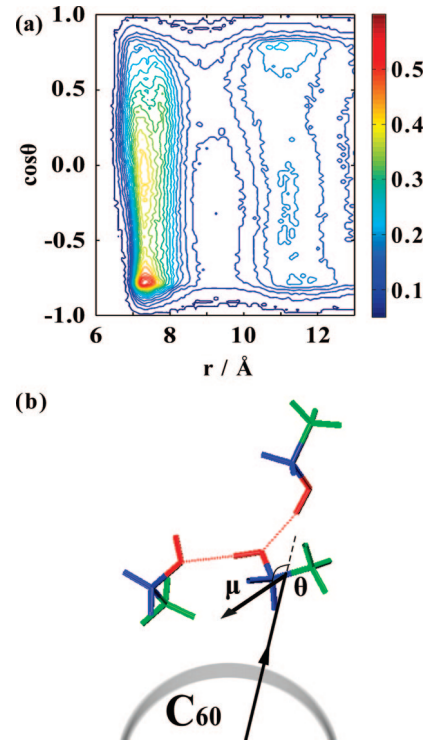

Figure 2. (a) Two-dimensional radial distribution function, $g(r, \cos\theta)$, in which r represents the distance between the COMs of C_{60} and ethanol, and θ denotes the angle between the vector from COM of C_{60} to ethanol and the dipole moment vector of the ethanol molecule. (b) Three representative orientations of ethanol molecules around the central C_{60}.

ethanol molecules around the C_{60} form a clathrate-like structure, which may stabilize the central C_{60} in ethanol solution.

The condensed-phase properties of ethanol are strongly influenced by the hydrogen-bond network. Thus, we analyzed the hydrogen-bonding distribution of the system by investigating the detailed distribution of the O−O distance and the smallest O···O−H angle of the tagged ethanol pairs. The distance/angular distribution, $g(r, \theta)$, for ethanol molecules in or between the solvation shells around the central C_{60} are employed for all ethanol molecule pairs classified by solvation shells. Each solvation shell corresponds to the ethanol layer between the minima of the COM RDF shown in Figure 1a. Figure 3a−g shows $g(r, \theta)$ within the first, second, third, and fourth solvation shells (S1−S1, S2−S2, S3−S3, S4−S4), as well as $g(r, \theta)$ between the first and the second solvation shells (S1−S2), the second and third solvation shells (S2−S3), and the third and fourth solvation shells (S3−S4), respectively. The correlation between two ethanol molecules within the distance between 2.5 and 3.2 Å and θ between 0 to 30° is due to the hydrogen-bond formation between the neighboring ethanol. The weak peaks at $4.6 \text{ Å} < r < 5.2 \text{ Å}$ and $20° < \theta < 40°$ denote the contact but not hydrogen-bonded ethanol molecules, as depicted in Figure 3h. Such structure is very similar to that of the water molecules surrounding a hydrophobic solute.[21,50] The very weak peak at ca. $r = 6.0$ Å, $\theta > 60°$ is comparable to Jorgensen's simulation of liquid ethanol, and the whole three peaks may indicate a U-shaped chain.[29] The contacted but not hydrogen-bonded ethanol molecules exhibit a long-range correlation, which may also contribute to an extended solvation structure around the central C_{60}.

In order to investigate the density of the hydrogen-bond network near the central C_{60}, we studied the hydrogen-bond

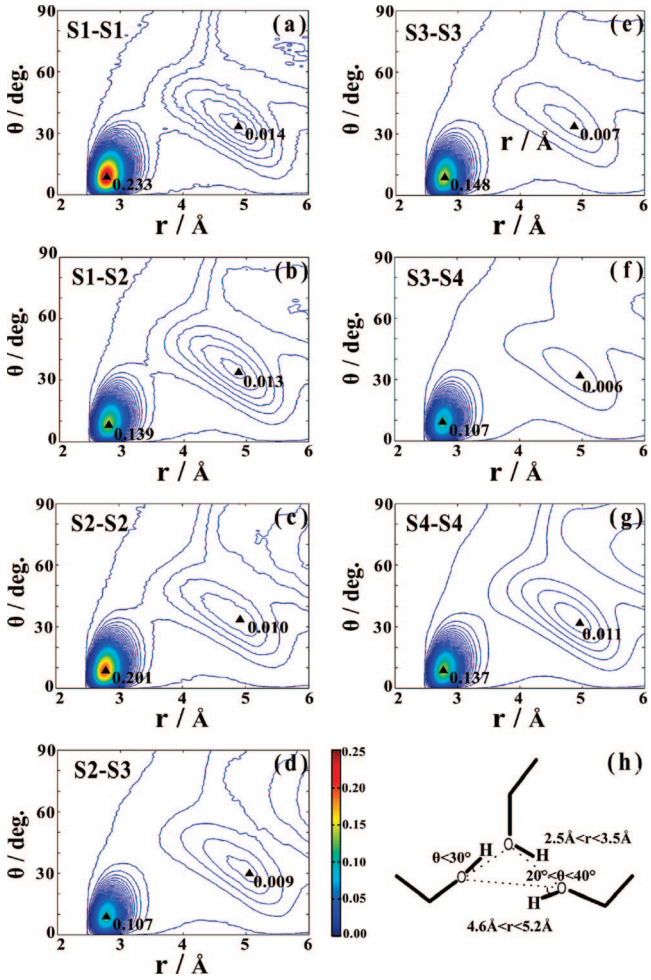

Figure 3. Two-dimensional O−O distance/O···O−H minimum angle distribution, $g(r, \theta)$, of the ethanol molecule pairs between and within different solvation shells around the central C_{60} molecule. (a) S1−S1; (b) S1−S2; (c) S2−S2; (d) S2−S3; (e) S3−S3; (f) S3−S4; (g) S4−S4. (h) Three body interaction among the ethanol molecules.

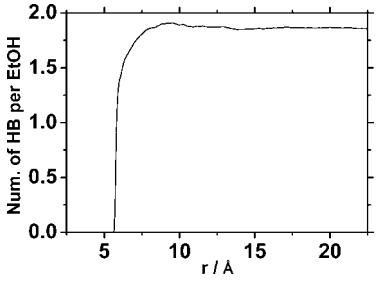

Figure 4. Hydrogen-bonding profile for the number of hydrogen-bonds per ethanol molecule versus the distance between the COM of C_{60} and the oxygen atom of ethanol.

profile versus the distance between the COM of C_{60} and ethanol. We adopted the geometrical definition of hydrogen-bond which has also been adopted in the previous simulations,[25,51] i.e., r(O−O) ≤ 3.5 Å, ∠ O···O−H ≤ 30°, and r(H−O) ≤ 2.5 Å. This definition is also consistent with the area of the main peak in the two-dimensional distance/angular RDF contour shown in Figure 3. The number of hydrogen-bonds per ethanol molecule versus distance between the COM of ethanol and C_{60} is shown in Figure 4. There is about 1.8 hydrogen-bonds per ethanol molecule in the solution, which is comparable to the previous simulation of liquid ethanol[29] and less than the number of hydrogen-bonds per water in the simulation of C_{60} in aqueous

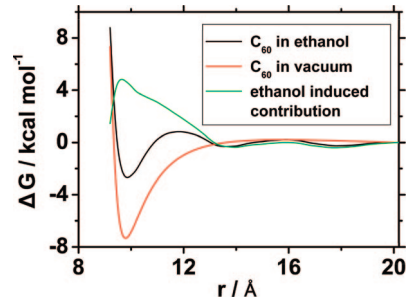

Figure 5. Potential of mean force of the fullerene versus distance between the COMs of two fullerene molecules in ethanol solution. The distance extends from 9.2 Å to 20.2 Å. The PMF is shifted to zero at the distance 20.2 Å. The black line represents the PMF of fullerene molecules in ethanol, the red line represents the PMF of fullerene molecules in vacuum, and the green line is the solvent contribution to the PMF.

solution.[25,46,52] The number of hydrogen-bonds per ethanol molecule decrease in the area near the surface of the central C_{60}. It is due to the curvature of the surface of the hydrophobic C_{60}, which hinders the formation of hydrogen-bonds between the neighboring ethanol molecules. From the CDF shown in Figure 1a (dashed line), there are few ethanol molecules in that area, and this tendency is not overwhelming in the ethanol solution. If we weighted this curve by RDF, it is obvious that the number of hydrogen-bonds per certain volume is notably enhanced because of the enhanced density of the ethanol molecules in S1. It is also supported by the angular/distance RDF in Figure 3a, in which the main peak in S1 is most intense. Therefore, the large density of the hydrogen-bond near the hydrophobic solute is due to the aggregation of ethanol rather than the enhancement of the number of hydrogen-bonds per ethanol. Such a hydrogen-bond network enwraps the central C_{60} and forms a clathrate-like structure.

3.2. Potential of Mean Force and Spatial Distribution of Ethanol. To investigate the association of the contact C_{60} pair and the stability of the aggregated fullerene particle in ethanol solution, we calculated the potential of mean force (PMF), as shown in Figure 5. The first minimum of the PMF is at ca. 9.8 Å between the COMs of two C_{60} molecules, which is comparable to the previous PMF calculation of fullerene in water.[26] Apart from that first minimum, there are two additional shallow minima at 13.6 Å and 17.8 Å, respectively. We explored the number of ethanol molecules in the intersolute region between two C_{60} molecules with the distance of 9.8 Å and found no ethanol molecule during the 2 ns MD simulation for the PMF production run. The free energy well at about 9.8 Å indicates that the C_{60} molecules tend to spontaneously aggregate in the ethanol solution, which is supported by the experiment of the measurement of the solubility of C_{60} in ethanol solution,[53] though the screening effect of the ethanol molecules contributes to separate and enwrap the C_{60} molecules. The depth of the first minimum in PMF is ca. 2.8 kcal/mol, which is shallower than the PMF of c.a. 4.2 kcal/mol of C_{60} in water reported by Smith and co-workers.[27] Therefore, it is easier for C_{60} to flee out of the potential well in ethanol than in aqueous solution.

In order to investigate the solvent contribution, we calculated the potential of mean force of two C_{60} molecules in vacuum, and the solvent-induced contribution was obtained from subtracting the fullerene direct interaction in vacuum from the PMF of C_{60} molecules in ethanol solution. The results are shown in Figure 5 in red and green lines, respectively, altogether with the PMF in ethanol solution. It can be seen that the contribution to the PMF by the ethanol solvent is purely a repulsion effect,

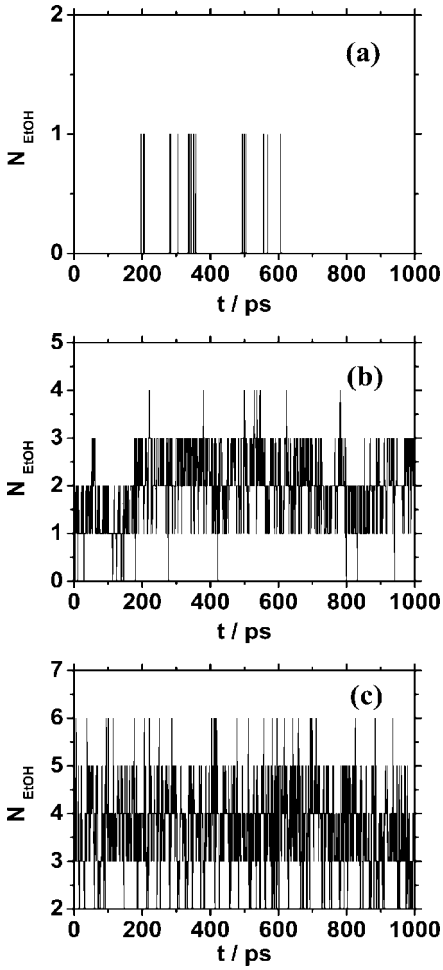

Figure 6. Instantaneous number of ethanol molecules in the intersolute region between two C_{60} molecules versus time. The number of ethanol molecules between two fullerene molecules within the separation of 10.2 Å (a), 13.4Å (b), and 17.8 Å (c), respectively.

which agrees with Smith's work on C_{60} in water,[27,46] as well as Choudhury and Pettitt's work on graphene in water.[43,54] It is notable that the repulsion induced by ethanol is much larger than that induced by water. Therefore, the spontaneous aggregation of C_{60} in the ethanol solution is due to direct van der Waals interaction between the C_{60} molecules. The enhanced repulsion effect indicates that C_{60} is easier to be dissolved in the ethanol solution, in agreement with the fact that the solubility of C_{60} molecules in ethanol is larger than in water.[53]

We also examined the number of ethanol molecules and their orientations in and near the intersolute area between two C_{60} molecules with all simulated distances to observe the solvent structure corresponding to the PMF. The ethanol molecules in the intersolute area are those with at least one of the functional groups, such as methyl or hydroxyl, penetrating into the intersolute area. As C_{60} molecules approach each other, the steric effect of C_{60} makes the intersolute area unavailable for many solvent molecules.[43] There is no molecule in the intersolute area when the COM distance between two C_{60} molecules is shorter than 10.2 Å. The instantaneous number of ethanol molecules in the intersolute area versus time within distances of 10.2 Å, 13.6 Å, and 17.8 Å are shown in Figure 6a, 6b, and 6c, respectively. Figure 6a shows the instantaneous number of ethanol molecules in the intersolute area at a critical distance between the COM of two fullerene molecules. The detailed orientation of the ethanol molecules near the intersolute area can be seen in Figure 7a, which is a snapshot of the system

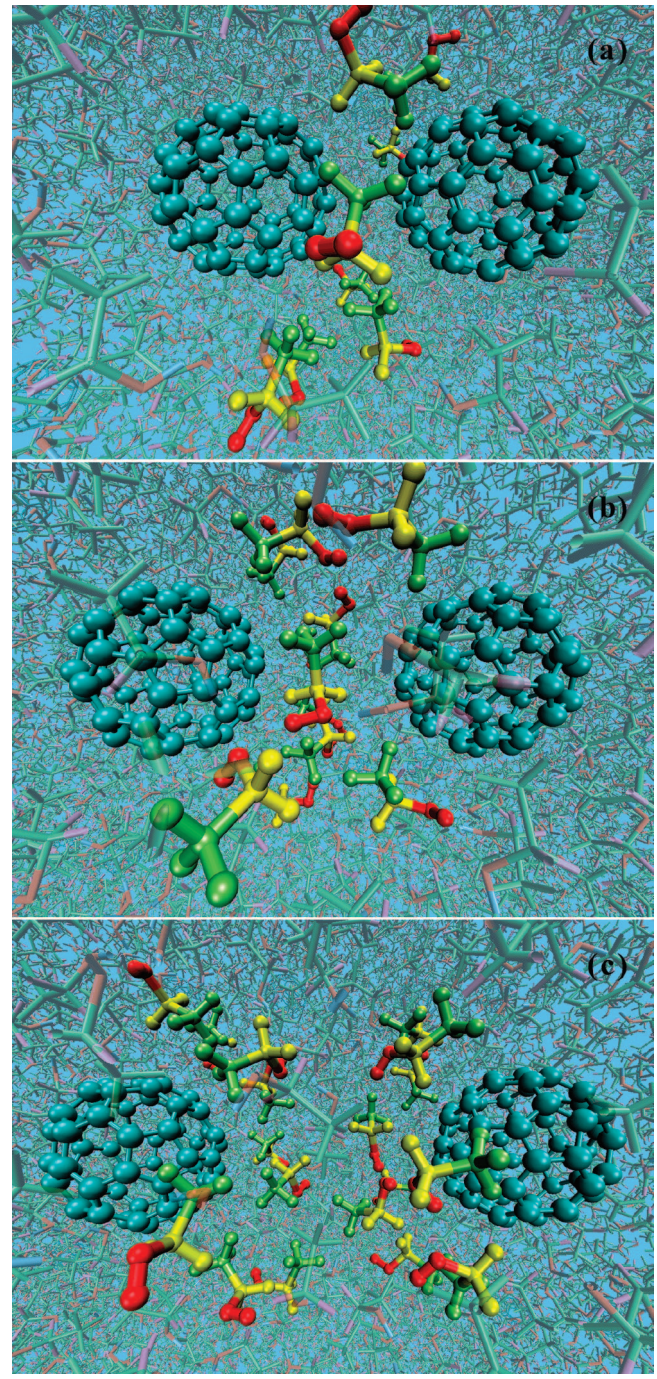

Figure 7. Snapshots of ethanol molecules in the intersolute region between two C_{60} molecules with fixed distances: (a) 10.2 Å; (b) 13.4 Å; (c) 17.8 Å.

obtained at the end of the PMF calculation with two C_{60} molecules separated by 10.2 Å. Most ethanol molecules have their alkyl groups pointing toward the surface of C_{60} molecules in order to have the hydroxyl groups pointing outward and maintain a hydrogen-bond network around the fullerene C_{60}. The instantaneous number of ethanol molecules shown in Figure 6b corresponds to the first shallow minimum in the PMF. The ethanol molecules penetrate into the intersolute area and form a layer of ethanol molecules, which hinder the direct contact of C_{60} molecules. By analyzing the trajectory accumulated in the PMF calculations, we find the methyl groups rather than hydroxyl groups of ethanol molecules tend to penetrate into the intersolute area when the two fullerene molecules are in relatively close contact. We can see directly in Figure 7b that

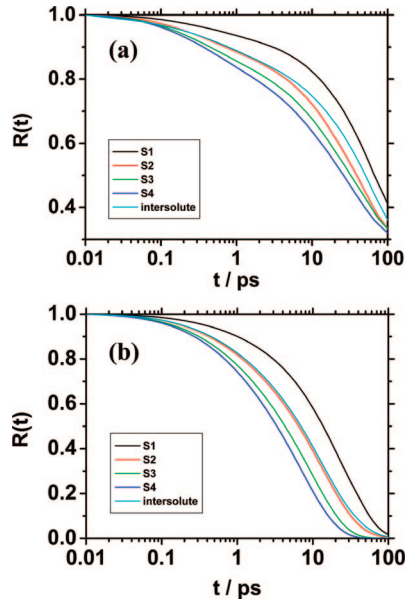

Figure 8. Cage correlation function, $R(t) = \langle\theta_i(t)\theta_i(0)\rangle/\langle\theta_i(0)\theta_i(0)\rangle$, of the ethanol molecules in S1 (black), S2 (red), S3 (green), and S4 (blue), respectively. (a) $\theta_i(t)$ represents the delta function; (b) $\theta_i(t)$ represents the heaviside step function.

the ethanol molecules near the intersolute area tend to reorientate themselves to fit both the C_{60} molecules and the center ethanol molecule penetrating into the intersolute area. If the distance between two fullerene molecules is long enough, two integrated ethanol layers are formed. The orientation of the ethanol molecules around two C_{60} molecules are shown in Figure 7c. It is corresponding to the second shallow minima of the PMF with the two C_{60} molecules separated by 17.8 Å, which is similar to Sasai's simulation of fullerene and water.[26] The ethanol molecules tend to enwrap two C_{60} molecules and form two clathrate-like structures. Such arrangement looks like the overlap of two independent clathrate-like clusters that interact with each other.

3.3. Dynamic Properties of the Solvation Shells. We employed several time correlation functions to study the dynamic properties of the solvation shells around the central C_{60} molecule. The occupation time of the ethanol molecules in different solvation shells can be evaluated by the cage correlation function of the ethanol molecules, i.e. $R(t) = \langle\theta_i(t)\theta_i(0)\rangle/\langle\theta_i(0)\theta_i(0)\rangle$, in which $\theta_i(t)$ represents the delta function, i.e., $\theta_i(t) = 1$ if at time t the COM of the ith ethanol molecule is in a specific solvation shell and $\theta_i(t) = 0$ otherwise. We also demonstrate cage correlation function with a different definition, in which $\theta_i(t)$ represents a heaviside step function, i.e., $\theta_i(t) = 1$ for the ith ethanol molecule in a specific solvation shell at t, and $\theta_i(t) = 0$ for any $t \geq t_1$, if at $t = t_1$ the ith ethanol molecule flees out of the solvation shell. The difference between the two definitions is that the second one excludes the oscillation of ethanol molecules between the neighboring shells. Figure 8a and 8b show $R(t)$s of the above two definitions, respectively. It can be concluded that the relaxation of the heaviside $\theta_i(t)$ definition is faster than that of the delta $\theta_i(t)$ definition. The knee at ~1 ps in Figure 8a denotes the oscillation of the ethanol molecules, initially in a specific solvation shell, which then flee out of it and re-enter. Thus, the oscillation of the ethanol molecules in the neighboring shell is quite frequent. In all the correlations of the above two different definitions, the relaxation of the ethanol molecules in the S1 decays more slowly than those in the other three solvation shells. In addition, we find

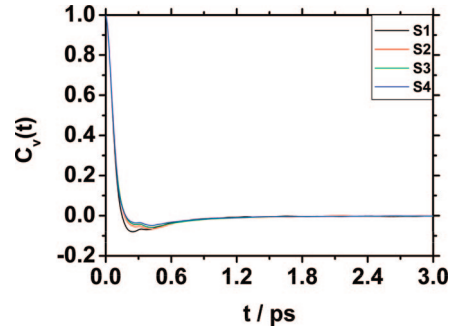

Figure 9. Velocity autocorrelation functions, $C_v(t)$, of the ethanol molecules in S1 (black), S2 (red), S3 (green), and S4 (blue), respectively.

that the relaxation time of the solvation shells is much longer than that of the water−fullerene system. The slower relaxation of ethanol is partly due to a diffusion of ethanol slower than that of water.[55,56] Moreover, the ethanol molecules reorient themselves to have their nonpolar tails pointing toward the surface of fullerene as well as the hydrophilic head pointing outward from the fullerene surface. Such structure is better to maintain the hydrogen-bond network and stabilizes the solvation shells.

Utilizing the same definition of the intersolute molecules in Figure 6, we analyzed the cage correlation for the ethanol molecules in the intersolute area between the two C_{60} molecules separated at a distance of 13.6 Å, which corresponds to the first shallow minimum of the PMF shown in Figure 5. The correlation functions, calculated by the same definitions for the ethanol molecules in different solvation shells, with an additional constraint on the molecules in the intersolute area, are also shown in Figure 8a and 8b, respectively. The relaxation of the ethanol molecules in the intersolute area is faster than those ethanol molecules in S1 but slower than the ethanol molecules in other solvation shells. This relaxation behavior is similar to the relaxation of water in the intersolute area between two C_{60} molecules.[23] Since additional constraint is applied on such a correlation function, it is reasonable to observe faster than S1 relaxation.[23] Indeed, the intersolute molecules resemble the molecules in the first solvation shell, and the much slower relaxation compared to S4 indicates that the intersolute molecules contribute to the metastability of the C_{60} molecules separated at this distance.

The velocity autocorrelation function (VACF), a sensitive character of the solvation shells around the central C_{60}, is defined as $C_v(t) = \langle\boldsymbol{v}_i(t)\cdot\boldsymbol{v}_i(0)\theta_i(t)\rangle/\langle\boldsymbol{v}_i(0)\cdot\boldsymbol{v}_i(0)\rangle$. In this function, $\boldsymbol{v}_i(t)$ is the instantaneous COM velocity of the ith ethanol molecules and $\theta_i(t) = 1$ if at time t the COM of the ith ethanol molecule in a certain solvation shell, and $\theta_i(t) = 0$ otherwise. The VACFs shown in Figure 9 are similar to the previous simulation of water around the central fullerene C_{60},[23] while the relaxation is slower. The negative value of $C_v(t)$ at ca. 0.2 ps for the solvation shells is mainly due to the rebound of the solvent molecules from the shell of their neighbor molecules.[57,58] It can be seen that the rebound in S1 is more pronounced than the other solvation shells. Therefore, the cage effect rising from the solute−ethanol interaction within S1 is stronger than in other solvation shells. The difference between the VACFs of the ethanol molecules in the inner solvation shells and in the outer solvation shells is similar to the VACFs of the ethanol molecules in the lower and higher temperatures.[59] Such similar phenomena are found in other simulations about the water in nanoscale confinement.[60,61] Thus, the ethanol molecules in S1 show a supercooled behavior

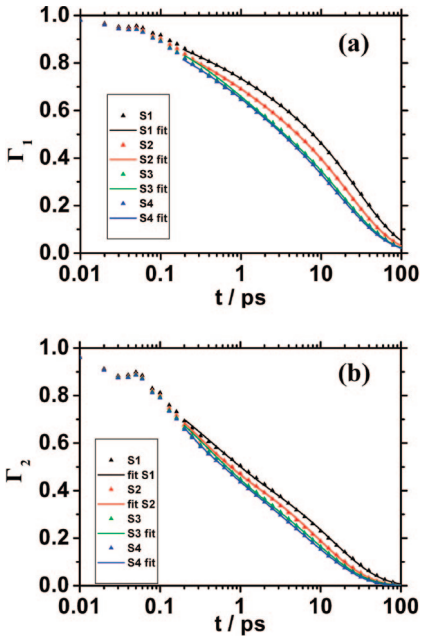

Figure 10. Reorientational correlation functions, $\Gamma_l(t)$, of the ethanol molecules in four solvation shells. (a) First rank reorientational correlation function, $\Gamma_1(t)$ (triangles), and KWW function fits (line) for ethanol molecules in S1 (black), S2 (red), S3 (green), and S4 (blue), respectively; (b) second rank reorientational correlation function, $\Gamma_2(t)$ (triangles), and KWW function fits (line) for ethanol molecules in S1 (black), S2 (red), S3 (green), and S4 (blue), respectively.

TABLE 1: Fitting Parameters for First Rank Reorientational Correlation Function by the KWW Function

solvation shell	A	τ_1^s (ps)	β_1^s	B	τ_1^l (ps)	β_1^l
S1	0.29	0.55	0.50	0.71	29.10	0.78
S2	0.34	0.55	0.50	0.66	23.30	0.77
S3	0.34	0.51	0.63	0.66	18.04	0.72
S4	0.34	0.45	0.53	0.66	16.67	0.70

TABLE 2: Fitting Parameters for Second Rank Reorientational Correlation Function by the KWW Function

solvation shell	A	τ_2^s (ps)	β_2^s	B	τ_2^l (ps)	β_2^l
S1	0.50	0.28	0.57	0.50	14.50	0.75
S2	0.40	0.25	0.99	0.60	10.88	0.66
S3	0.45	0.25	0.82	0.55	8.23	0.71
S4	0.42	0.29	0.80	0.57	7.56	0.69

because of the inducement of the central C_{60}. With the elongation of the distance between the COM of C_{60} and ethanol, the VACF for ethanol is comparable to that for liquid ethanol at 298 K.[59]

In order to study the orientational dynamics of the ethanol molecules in different solvation shells, first and second rank reorientational correlation functions, $\Gamma_l(t) = \langle P_l(\boldsymbol{\mu}_i(t))\boldsymbol{\mu}_i(0)\rangle$, are shown in Figure 10a and 10b, respectively. In the above expression, P_l for $l = 1, 2$ denotes the first and second order Legendre polynomial, and $\boldsymbol{\mu}_i$ represents the unit vector along the dipole moment of the ethanol molecule. Kohlrausch−Williams−Watts (KWW) function, i.e., $\Gamma_l(t) = A\exp(-t/\tau_l^s)^{\beta_l^s} + B\exp(-t/\tau_l^l)^{\beta_l^l}$,[23,24,55] is employed to fit $\Gamma_l(t)$, with the fitted parameters listed in Table 1 and 2, respectively, for $\Gamma_1(t)$ and $\Gamma_2(t)$. The initial bumps in Figure 10, with time shorter than 0.2 ps, show the ultrafast motion due to the librational motion of hydrogen-bond. Since the dipole moment of the ethanol molecule is largely contributed by the OH group, such a bump is closely related to the intermolecular hydrogen-bond vibrations, as will be discussed below for the hydrogen-bond dynamics. Such ultrafast motion cannot be fitted by the KWW function, which describes the long time relaxation. Apart from the initial ultrafast motion, it can be seen that the KWW function well fits the reorientational correlation functions longer than 0.2 ps. The relaxation includes two processes, i.e., a fast step followed by a slow step. The fast step, with the time scale of 0.45−0.55 ps for $\Gamma_1(t)$ and 0.25−0.30 ps for $\Gamma_2(t)$, may be attributed to the interoxygen atom vibration of the ethanol molecules, which also appears in the previous MD simulation of water[62] and experimental measurement of the reorientation and fluctuation of the water.[63] Therefore, the short relaxation time τ_l^s of such motion for the ethanol molecules in four solvation shells shows approximately the same time scale. The long time relaxation, characterized by relaxation time τ_l^l, is attributed to the complete relaxation of reorientation of the ethanol molecules in different solvation shells. It can be seen that τ_l^l decreases with outer solvation shells for both $\Gamma_1(t)$ and $\Gamma_2(t)$. The difference of the resident time of the reorientation of the ethanol molecules in outer solvation shells is not as much as that for ethanol molecules in the inner solvation shells for both the first and second rank dipole correlation functions. Consequently, it can be seen that the fullerene molecule slows down the reorientation dynamics of the ethanol molecules close to it, similar to that of the simulation of the fullerene in aqueous solution.[23,24,55] The relaxation of $\Gamma_2(t)$ in all the four solvation shells is faster than $\Gamma_1(t)$. It can be estimated from Tables 1 and 2 that τ_1^l/τ_2^l is approximately 2.0, 2.1, 2.2, and 2.2, respectively, for S1, S2, S3, and S4. For an isotropic rotation, $\tau_1^l/\tau_2^l = 3$.[64] The smaller τ_1^l/τ_2^l for the solvation shells, especially for S1, indicates the hindered reorientation for the ethanol molecules.

Dynamic properties of the condense-phase ethanol depend much on the formation and break of the hydrogen-bonds, which could be detected by experiment[65] and MD simulation.[30,66,67] We investigated the fluctuation of the hydrogen-bonds between ethanol pairs in certain solvation shell by the correlation function $C_h(t) = \langle h(t)h(0)\rangle/\langle h(0)h(0)\rangle$, in which $h(t) = 1$ if the tagged ethanol pair in certain solvation shells is hydrogen-bonded at t and $h(t) = 0$ otherwise, same as that defined in the previous simulation of water solution.[68,69] The initial bump shown in the inset of Figure 10a is due to the librational motion with the time-span shorter than 0.2 ps, which is familiar in aqueous solution.[68] We find the relaxation of the hydrogen-bonds between ethanol molecules within the first solvation shell (S1−S1) is slower than the relaxation in any other solvation shell. The hydrophobic nature of the C_{60} surface makes most of the ethanol molecules in S1 have the hydroxyl group pointing outward and maintains a hydrogen-bond network at the outer boundary of S1. The relaxation of the hydrogen-bonds between ethanol molecules in S1 mainly represents the dynamic properties of this hydrogen-bond network. The curves shown in Figure 11a indicates the stable clathrate-like structure due to the stable hydrogen-bond network. A similar phenomenon was also found in the previous simulation of nanoconfinement that makes the solvent molecules have slower hydrogen-bonding relaxation.[61] The stable hydrogen-bonds hinder the diffusion of the molecules[69] and thus contributes to the stabilization of the inner solvation shells. The relaxation of the hydrogen-bonds correlates well within the solvation shells and becomes faster for the outer solvation shells as the configuration of those ethanol molecules becomes less ordered.

The breakage of the hydrogen-bonds is caused by reorientation or pair mutual diffusion of the ethanol molecules. We examined the reorientational contribution to the breakage of hydrogen-bonds, which is denoted by $n_h(t) = \langle h(0)[1 - h(t)]H(t)\rangle/\langle h(0)h(0)\rangle$, in which $H(t) = 1$ if the distance between

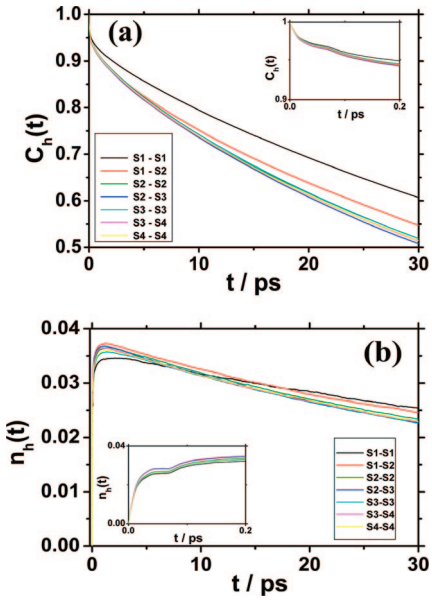

Figure 11. (a) Hydrogen-bond autocorrelation function, $C_h(t)$; (b) reorientation of hydroxyl group induced breakage of hydrogen-bonds, $n_h(t)$, of the hydrogen-bonded ethanol molecule pairs within and between different solvation shells. S1−S1 (black); S1−S2 (red); S2−S2 (green); S2−S3 (blue); S3−S3 (cyan); S3−S4 (pink); S4−S4 (yellow). The insets show $C_h(t)$ and $n_h(t)$ within 0.2 ps, respectively.

the oxygen atoms in the pairwise ethanol molecules is shorter than 3.5 Å at time t and $H(t) = 0$ otherwise.[68−70] Thus, $n_h(t)$ describes the breakage of the hydrogen-bond at time t purely attributed to the reorientation of the hydroxyl groups of the initially hydrogen-bonded ethanol pair. After the breakage of the hydrogen-bonds by the reorientation between the neighboring ethanol molecules, these ethanol molecules will mutually diffuse away. This whole process may be regarded as a two-step continuous reaction. The value of the peak in $n_h(t)$ may also partially represent the relative reaction ratio of these two reactions. We can see from Figure 11b that $n_h(t)$ is much smaller than that for aqueous solution over the whole time window investigated.[69] Therefore, the reorientation of the hydroxyl group of the tagged ethanol pair contributes less to the breakage of hydrogen-bond in ethanol solution because the reorientation of ethanol molecules is slower than that of the water molecules. We also find that the value of the peak in $n_h(t)$ for the ethanol molecules in S1 is relatively smaller than those for ethanol molecules in other solvation shells. It indicates that the hydrogen-bond network of the clathrate-like structure hinders the reorientation of the hydroxyl groups of the hydrogen-bonded ethanol pairs. The behavior of $n_h(t)$ at a long time scale is determined by the rotation diffusion of the solvent molecules.[70] It is notable that $n_h(t)$ for ethanol in S1 at a longer time, i.e., 18 ps, is larger than those in the other solvation shells. Therefore, the rotation of the ethanol molecules in S1 is slower than that of the ethanol molecules in other solvation shells.

4. Conclusion

We studied the structure and dynamic properties of ethanol around fullerene C_{60} by molecular dynamics simulation. The radial distribution functions of the system are much extended, and four solvation shells surrounding the central C_{60} molecule can be identified. Because of the curvature and hydrophobic nature of the C_{60} surface, the ethanol molecules in S1 tend to have their hydroxyl groups pointing outward to maintain the hydrogen-bond network. The distribution of the dipole moment of the ethanol molecules indicates that some ethanol molecules in S1 have their oxygen atoms exposed as hydrogen-bond acceptors. The interconnection between S1 and S2 is mainly governed by the hydrogen-bonds, which makes the ethanol molecules in S2 have a distinct orientation where most of the molecules have their hydroxyl group pointing inward. The orientations of the ethanol molecules in the outer solvation shell gradually become isotropic. The PMF of the system shows that the C_{60} molecules tend to spontaneously aggregate in ethanol solution, although the ethanol molecules may separate and enwrap the C_{60} molecule and form the clathrate-like structure. The orientations of the ethanol molecules in the intersolute area tend to have the hydroxyl group pointing outward to maintain a hydrogen-bond network that enwraps both of the C_{60} molecules, when the distance between COM of two C_{60} molecules is relatively short. With the elongation of the distance between two C_{60} molecules, the ethanol molecules tend to enwrap the individual C_{60} molecule. The inducement of the central C_{60} molecule makes the ethanol molecules form a clathrate-like structure. Such structure slows down the dynamic properties of the ethanol molecules in the inner solvation shell, which is comparable to the supercooled behavior of the ethanol liquid. With an increase in distance between the ethanol molecules and the central C_{60}, the dynamic properties of the ethanol molecules approaches the room temperature ethanol solution. The local ordered clathrate-like structure also affects the dynamic properties of the hydrogen-bonds in the inner solvation shells. We find the fluctuation of the hydrogen-bonds in S1 is much slower than that in other solvation shells, which makes S1 more stable than the other solvation shells.

This study shows that amphiphilic ethanol solution around the target C_{60} molecule has many similarities compared with the aqueous solution. Because the C_{60} molecule breaks the hydrogen-bond network in the solution, the solvent molecules reorientate around the C_{60} molecule and form a highly ordered clathrate-like structure with slowed dynamic properties. However, there are some differences in the solvent structure and dynamics properties because of the special hydrophobic tail of the amphiphilic ethanol molecule. The hydroxyl groups of the solvent molecule would be repelled from the surface of the C_{60} molecule because of the hydrophobic properties as well as the curvature of C_{60}. For water, the whole molecule is pushed away, while for ethanol, the molecule tends to adopt a specific orientation with the hydrophobic tail pointing toward the C_{60} surface to form a clathrate-like structure. The orientation of the ethanol molecules near the C_{60} molecule further affect the other solvation shell structures and result in a more intense RDF compared with that for aqueous solution. Such orientation also increases van der Waals interactions between C_{60} and ethanol molecules and stabilizes the clathrate-like structure. Both ethanol and water contributions to the PMF are a repulsion effect, but the ethanol solution brings a larger repulsion contribution.

Acknowledgment. This research is supported by the NSFC (No. 20503013). T.Y.'s participation in the project was also partially sponsored by Renshi Chu startup funding of Nankai University and the scientific research foundation for the ROCS, Ministry of Education, China. The allocation of computer time from Institute of Scientific Computing at Nankai University is gratefully acknowledged.

References and Notes

(1) Minakata, S.; Tsuruoka, R.; Komatsu, M. *J. Am. Chem. Soc.* **2008**, *130*, 1536.
(2) Innocenzi, P.; Brusatin, G. *Chem. Mater.* **2001**, *13*, 3126.

(3) Voityuk, A. A.; Duran, M. *J. Phys. Chem. C* **2008**, *112*, 1672.
(4) Bond, A. M.; Miao, W.; Raston, C. L.; Ness, T. J.; Barnes, M. J.; Atwood, J. L. *J. Phys. Chem. B* **2001**, *105*, 1687.
(5) Noon, W. H.; Kong, Y.; Ma, J. *Proc. Natl. Acad. Sci. U.S.A.* **2002**, *99*, 6466.
(6) Friedman, S. H.; Decamp, D. L.; Sijbesma, R. P.; Srdanov, G.; Wudl, F.; Kenyon, G. L. *J. Am. Chem. Soc.* **1993**, *115*, 6506.
(7) Tokuyama, H.; Yamago, S.; Nakamura, E.; Shiraki, T.; Sugiura, Y. *J. Am. Chem. Soc.* **1993**, *115*, 7918.
(8) Nakamura, E.; Isobe, H. *Acc. Chem. Res.* **2003**, *36*, 807.
(9) Zheng, M.; Jagota, A.; Semke, E. D.; Diner, B. A.; Mclean, R. S.; Lustig, S. R.; Richardson, R. E.; Tassi, N. G. *Nat. Mater.* **2003**, *2*, 338.
(10) Nel, A.; Xia, T.; Mädler, L.; Li, N. *Science* **2006**, *311*, 622.
(11) Khabashesku, V. N.; Billups, W. E.; Margrave, J. L. *Acc. Chem. Res.* **2002**, *35*, 1087.
(12) Sun, Y.-P.; Fu, K.; Lin, Y.; Huang, W. *Acc. Chem. Res.* **2002**, *35*, 1096.
(13) Pratt, L. R.; Pohorille, A. *Chem. Rev.* **2002**, *102*, 2671.
(14) Brant, J.; Lecoanet, H.; Notze, M.; Wiesner, M. *Environ. Sci. Technol.* **2005**, *39*, 6343.
(15) Maibaum, L.; Dinner, A. R.; Chandler, D. *J. Phys. Chem. B* **2004**, *108*, 6778.
(16) Tanford, C. *Science* **1978**, *200*, 1012.
(17) Lum, K.; Chandler, D.; Weeks, J. D. *J. Phys. Chem. B* **1999**, *103*, 4570.
(18) Chandler, D. *Nature* **2005**, *437*, 640.
(19) Huang, D. M.; Geissler, P. L.; Chandler, D. *J. Phys. Chem. B* **2001**, *105*, 6704.
(20) Chandler, D. *Nature* **2007**, *445*, 831.
(21) Weiss, D. R.; Raschke, T. M.; Levitt, M. *J. Phys. Chem. B* **2008**, *112*, 2981.
(22) Stillinger, F. H. *J. Solution Chem.* **1973**, *2*, 141.
(23) Choudhury, N. *J. Phys. Chem. C* **2007**, *111*, 2565.
(24) Choudhury, N. *J. Phys. Chem. B* **2007**, *111*, 10474.
(25) Choudhury, N. *J. Chem. Phys.* **2006**, *125*, 034502.
(26) Hotta, T.; Kimura, A.; Sasai, M. *J. Phys. Chem. B* **2005**, *109*, 18600.
(27) Li, L.; Bedrov, D.; Smith, G. D. *Phys. Rev. E* **2005**, *71*, 011502.
(28) Kim, H.; Bedrov, D.; Smith, G. D. *J. Chem. Theory Comput.* **2008**, *4*, 335.
(29) Jorgensen, W. L. *J. Am. Chem. Soc.* **1981**, *103*, 345.
(30) Padrò, J. A.; Saiz, L.; Guàrdia, E. *J. Mol. Struct.* **1997**, *416*, 243.
(31) Malaspina, T. *J. Phys. Chem. B* **2007**, *111*, 11935.
(32) Chen, J.; Rao, A. M.; Lyuksyutov, S.; Itkis, M. E.; Hamon, M. A.; Hu, H.; Cohn, R. W.; Eklund, P. C.; Colberlt, D. T.; Smalley, R. E.; Haddon, R. C. *J. Phys. Chem. B* **2001**, *105*, 2525.
(33) Sathish, M.; Miyazawa, K. *J. Am. Chem. Soc.* **2007**, *129*, 13816.
(34) Alargova, R. G.; Deguchi, S.; Tsujii, K. *J. Am. Chem. Soc.* **2001**, 123.
(35) Deguchi, S.; Alargova, R. G.; Tsujii, K. *Langmuir* **2001**, *17*, 6013.
(36) Deguchi, S.; Mukai, S.; Tsudome, M.; Horikoshi, K. *Adv. Mater.* **2006**, *18*, 729.
(37) Andrievsky, G. V.; Klochkov, V. K.; Bordyuh, A. B.; Dovbeshko, G. I. *Chem. Phys. Lett.* **2002**, *364*, 8.
(38) Lindahl, E.; van der Spoel, D. *J. Mol. Model.* **2001**, *7*, 306.
(39) Jorgensen, W. L.; Maxwell, D. S.; Tirado-Rives, J. *J. Am. Chem. Soc.* **1996**, *118*, 11225.
(40) Cornell, W. D.; Cieplak, P.; Bayly, C. I.; Gould, I. R.; Merz, K. M.; Ferguson, D. M.; Spellmeyer, D. C.; Fox, T.; Caldwell, J. W.; Kollman, P. A. *J. Am. Chem. Soc.* **1995**, *117*, 5179.
(41) Ryckaert, J. P.; Ciccotti, G.; Berendsen, H. J. C. *J. Comp. Phys.* **1977**, *23*, 327.
(42) Choudhury, N.; Pettitt, B. M. *J. Am. Chem. Soc.* **2007**, *129*, 4847.
(43) Choudhury, N.; Pettitt, B. M. *J. Am. Chem. Soc.* **2005**, *127*, 3556.
(44) Darden, T.; York, D.; Pedersen, L. *J. Chem. Phys.* **1993**, *98*, 10089.
(45) Berendsen, H. J. C.; Postma, J. P. M.; van Gunsteren, W. F.; DiNola, A.; Haak, J. R. *J. Chem. Phys.* **1984**, *81*, 3684.
(46) Li, L.; Bedrov, D.; Smith, G. D. *J. Chem. Phys.* **2005**, *123*, 204504.
(47) Howard, C. A.; Wasse, J. C.; Skipper, N. T.; Thompson, H.; Soper, A. K. *J. Phys. Chem. C* **2007**, *111*, 5640.
(48) Ludwig, R.; Appelhagen, A. *Angew. Chem., Int. Ed.* **2005**, *44*, 811.
(49) Hernández-Rojas, J.; Bretón, J.; Gomez Llorente, J. M.; Wales, D. J. *J. Phys. Chem. B* **2006**, *110*, 13357.
(50) Raschke, T. M.; Levitt, M. *Proc. Natl. Acad. Sci. U.S.A.* **2005**, *102*, 6777.
(51) Jedlovszky, P.; Brodholt, J. P.; Bruni, F.; Ricci, M. A.; Soper, A. K.; Vallauri, R. *J. Chem. Phys.* **1998**, *108*, 8528.
(52) Li, L.; Bedrov, D.; Smith, G. D. *J. Phys. Chem. B* **2006**, *110*, 10509.
(53) Heymann, D. *Carbon* **1996**, *34*, 627.
(54) Choudhury, N.; Pettitt, B. M. *J. Phys. Chem. B* **2006**, *110*, 8459.
(55) Li, Z.; Wang, Q.; Liu, Y.-C.; Zhang, L.-Z. *J. Chem. Phys.* **2006**, *125*, 10452.
(56) Zhang, C.; Yang, X. *Fluid Phase Equilib.* **2005**, *231*, 1.
(57) Choudhury, N.; Pettitt, B. M. *J. Phys. Chem. B* **2005**, *109*, 6422.
(58) Zichi, D. A.; Rossky, P. J. *J. Chem. Phys.* **1986**, *84*, 2814.
(59) Saiz, L.; Padrò, J. A. *J. Phys. Chem. B* **1997**, *101*, 78.
(60) Hummer, G.; Rasaiah, J. C.; Noworyta, J. P. *Nature* **2001**, *414*, 188.
(61) Kolesnikov, A. I.; Zanotti, J.-M.; Loong, C.-K.; Thiyagarajan, P.; Moravsky, A. P.; Loutfy, R. O.; Burnham, C. J. *Phys. Rev. Lett.* **2004**, *93*, 035503.
(62) Luzar, A.; Chandler, D. *Phys. Rev. Lett.* **1996**, *76*, 928.
(63) Loparo, J. J.; Fecko, C. J.; Eaves, J. D.; Roberts, S. T.; Tokmakoff, A. *Phys. Rev. B* **2004**, *70*, 180201.
(64) Shim, Y.; Kim, H. J. *J. Phys. Chem. B* **2008**, *112*, 11028.
(65) Kropman, M. F.; Bakker, H. J. *Science* **2001**, *291*, 2118.
(66) Kosztolányi, T.; Bakó, I.; Pálinkás, G. *J. Chem. Phys.* **2003**, *118*, 4546.
(67) Padrò, J. A.; Saiz, L.; Guàrdia, E. *Mol. Phys.* **1999**, *97*, 897.
(68) Luzar, A.; Chandler, D. *Nature* **1996**, *379*, 55.
(69) Xu, H.; Berne, B. J. *J. Phys. Chem. B* **2001**, *105*, 11929.
(70) Xu, H.; Stern, H. A.; Berne, B. J. *J. Phys. Chem. B* **2002**, *106*, 2054.

JP805894G